Photoelectron spectroscopy of para-benzoquinone cluster anions

*Golda Mensa-Bonsu, Mark R. Wilson, David J. Tozer, Jan R. R. Verlet**

Department of Chemistry, Durham University, Durham DH1 3LE, United Kingdom.

Abstract

The photoelectron spectra of para-benzoquinone radical cluster anions, $(p\text{BQ})_n^-$ (n = 2 – 4), taken at $h\nu$ = 4.00 eV are presented and compared the photoelectron spectrum of the monomer (n = 1). For all cluster, a direct detachment peak can be identified and the incremental increase in vertical detachment energy of ~0.4 eV n^{-1} predominantly reflects the increase in cohesion energy as the cluster size increases. For all clusters, excitation also leads to low energy electrons that are produced by thermionic emission from ground electronic state anionic species, indicating that resonances are excited at this photon energy. For n = 3 and 4, photoelectron features at lower binding energy are observed which can be assigned to photodetachment from $p\text{BQ}^-$ for n = 3 and both $p\text{BQ}^-$ and $(p\text{BQ})_2^-$ for n = 4. These observations indicate that the cluster dissociates on the timescale of the laser pulse (~5 ns). The present results are discussed in the context of related quinone cluster anions.

*j.r.r.verlet@durham.ac.uk

I. Introduction

Quinones are a class of cyclic diketone compounds which have significant biological relevance due to their ubiquitous role as an electron acceptor in nature. Of the various processes involving quinones, the function of ubiquinone and plastoquinone within the electron transport chains of respiration and photosynthesis, respectively, is particularly prominant.[1,2] Quinones have also been explored in replicating natural photosynthetic processes for the purpose of energy generation.[3,4] The central moiety common to all quinone derivatives[5] that is responsible for their electron accepting properties is benzoquinone,[6] with the *para*-benzoquinone (*p*BQ) structural isomer being the most common.[5] Owing to its simple structure and abundance in nature, *p*BQ can be viewed as an "electrophore" – a chemical moiety with an efficient electron acceptor ability.[7] This ability is closely related to the dynamics of the resonances of the *p*BQ anion, pBQ^{-}.[8,9] Consequently, much work has been carried out towards understanding the resonances of pBQ^{-}.[6–31] However, in nature and in many synthetic systems, quinones are often found as dimers[32,33] and this leads to the natural question: how do the resonance dynamics change in *p*BQ oligomer anions, $(pBQ)_n^{-}$? From a materials perspective, oligomer dynamics are of key importance in understanding bulk properties. Much less is known about the photophysics of such clusters. Here, we explore how the oligomerisation of the singly charged *p*BQ anion affects the photoelectron spectroscopy.

*p*BQ has a large positive electron affinity (1.860 ± 0.005 eV) and is therefore capable of forming stable anions.[8] As the anion formation process is mediated by temporary excited states of the anion (resonances), there have been many studies aimed at characterising the spectroscopy and resonances of pBQ^{-} and, moreover, to elucidate the photophysical processes involved in stable anion formation.[6,10,12–16,25,34] Schiedt and Weinkauf measured the photodetachment cross section of the jet-cooled radical anion within the 2.0 – 2.5 eV photon

energy range and identified several resonances above threshold.[8] At photon energies resonant with resonances, the dominant detachment pathway was an indirect autodetachment channel (as opposed to the direct detachment pathway). 2D photoelectron spectroscopy of the anion resonances of *p*BQ$^-$ have confirmed the presence of the previously reported ^2A_u shape resonance and the $^2B_{3u}$ Feshbach resonance, both at ~ 2.5 eV.[9,22] Time-resolved photoelectron spectroscopy and *ab initio* calculations were able to probe the decay mechanism of the resonances, which showed that internal conversion on a ~20 fs timescale was able to compete with autodetachment from the initially populated $^2B_{3u}$ resonance. This extremely fast decay provided an explanation of the efficiency of *p*BQ as an electron acceptor.[35] Prior to these works, Brauman *et al.* focused on finding evidence for a specific type of metastable doorway state in the electron attachment processes of radical benzoquinone: a dipole-bound state.[25] Although *para-* and *ortho*-benzoquinone have similar electronic structures, the dipole moments of the isomers differ significantly, and as such, only *o*BQ is capable of sustaining a dipole bound state. This difference was reflected in the photodetachment action spectra of the benzoquinones for which *o*BQ$^-$ showed resonances associate with the dipole-bound state, while *p*BQ$^-$ did not.[25]

In addition to experiments using the anion as a starting point, the resonances of *p*BQ$^-$ have been the subject of many electron scattering experiments.[10–21] In general, the photoelectron and photodetachment spectroscopy is in agreement with these studies, although positions of resonances differ because of the differing initial geometries. Finally, *p*BQ$^-$ resonances have also been the subject of several theoretical studies including scattering calculations and high-level electronic structure calculations.[7,26–31,33,36] Again, a generally consistent picture has emerged about the photophysics of the resonances of *p*BQ$^-$ that is in overall agreement with the experimental work using many different methodologies.

In contrast to the wealth of information regarding the spectroscopy and dynamics of *p*BQ$^-$, only a few studies have considered the clusters of related molecules. In electron scattering experiments, studying clusters is more challenging, as mass-selection of the initial neutral target is not possible. Experiments starting from anionic clusters do not suffer from this restriction. The group of Brauman studied the photodetachment spectroscopy of *para*-toluquinone dimer $(p\text{TQ})_2^-$.[24] In this, they found that a *bound* charge transfer state (called a charge-resonance state, but we avoid this nomenclature for clarity here) that was present at $h\nu \sim 1.9$ eV resulted in the dissociation of the cluster: $(p\text{TQ})_2^- + h\nu \rightarrow p\text{TQ} + p\text{TQ}^-$. Our group has also studied clusters of *para*-toluquinone $(\text{pTQ})_n^-$ ($n \leq 3$) by 2D photoelectron spectroscopy.[37] This showed some indirect evidence that the dimer dissociated above threshold, while the trimer revealed interesting valence to non-valence internal conversion dynamics near threshold, in which the non-valence state observed presented the first example of a predominantly correlation-bound state.[38] While *p*TQ can be viewed as a good approximation to *p*BQ, we were previously not able to produce *p*BQ cluster anions in the electrospray source.[9] Here, we have generated $(p\text{BQ})_n^-$ ($n \leq 4$) using a molecular beam source and we present its photoelectron spectroscopy at $h\nu = 4.00$ eV (310 nm). This shows the dimer does not undergo fragmentation following excitation, while the trimer and tetramer dissociate to give anionic and neutral fragments.

II. Experimental & Computational Details

The experimental setup has previously been discussed in detail elsewhere.[39] As such, only a brief summary is given here. Solid pBQ was heated to 113 °C in a pulsed Even-Lavie valve,[40] prior to the molecular vapour being expanded into vacuum using Ar as backing gas (3 bar). The resulting molecular beam was crossed by an electron beam (300 eV) at the throat

of the expansion. Ion packets containing $(p\text{BQ})_n^-$ ($n \leq 4$) were mass-selected using a Wiley-McLaren time-of-flight spectrometer[41] before being intersected by nanosecond laser pulses from a tuneable Nd:YAG pumped optical parametric oscillator. The resulting photoejected electrons were accelerated towards a position sensitive detector in a velocity map imaging spectrometer,[42,43] allowing the electron kinetic energy (eKE) of the photoelectrons to be determined. Photoelectron spectra were reconstructed from raw images using the polar onion peeling algorithm[44] and were calibrated using the known photoelectron spectrum of I^-. The spectra have a resolution of $\Delta eKE/eKE < 3\%$.

Computational methods were employed to elucidate the structure of the radical $(p\text{BQ})_n^-$ produced and probed in the experiment. First, the configurational space of $(p\text{BQ})_n^-$ was explored for $n = 2 – 4$ through a sequence of energy minimisation calculations using the SANDER functionality within the AMBER18 molecular dynamics package.[45] Although not a comprehensive analysis of configurational space, these calculations provided an indication of the dominant interactions, which govern the structure of the oligomer anion. Starting with the dimer, Restrained Electrostatic Potential (RESP) charges (HF/6-31G*) were assigned to one *p*BQ monomer (net –1 charge) and the other *p*BQ monomer remained neutral (zero net charge). For these two species, the minimisation calculations commenced from a series of 5000 random starting positions and orientations, in which the neutral monomer was positioned around the anionic monomer, distributed on spheres of radii between 3 and 15 nm. Minimisation calculations evolved from each of these starting positions using the Generalised Amber Force Field and RESP charges.[46] From this, a number of possible local minima were identified, which served as initial starting structures for Density Functional Theory (DFT) calculations. For $(p\text{BQ})_3^-$ and $(p\text{BQ})_4^-$, the minimisation procedure was extended to allow random starting configurations for three and four species, by placing two and three randomly oriented monomers around a central anionic *p*BQ.

DFT optimisation calculations were performed commencing from the AMBER minimised configurations at the ωB97XD/6-31+G* level of theory using Gaussian09.[47,48] This functional was specifically designed with an emphasis on non-bonded interactions. Minimum energy structures were confirmed using vibrational analysis. For comparative purposes, the optimised geometry of the radical monomer anion was also computed using DFT at the same level of theory.

III. Results & Analysis

A. Experimental

Photoelectron spectra were obtained for $(p\text{BQ})_n^-$ (n = 2 - 4) at $h\nu$ = 4.00 eV and were compared to that of $p\text{BQ}^-$, which had been measured at $h\nu$ = 4.20 eV. Note that the spectrum of $p\text{BQ}^-$ at 4.20 eV is almost identical as that at 4.00 eV (in terms of binding energy) and was taken at this photon energy to capture the triplet state of the neutral which served as an internal calibration.[23] The area-normalised spectra are displayed in Figure 1, where they have been plotted in terms of electron binding energy (eBE = $h\nu$ – eKE). The photoelectron spectrum of $p\text{BQ}^-$ shows a broad Gaussian-like feature centred around eBE ~ 2.2 eV. This band represents the direct detachment process in which an electron is instantaneously photoejected from the electronic ground state of the monomer anion to that of neutral *p*BQ. The large spectral width of the peak arises from the significant difference in geometry between the anion and neutral. By measuring the eBE at which the onset and maximum of the direct detachment band occurs, the adiabatic and vertical detachment energies (ADE and VDE), respectively, can be determined. For $p\text{BQ}^-$, this yields ADE = 1.85 ± 0.02 eV and VDE = 2.24 ± 0.02 eV. These values are in agreement with previous experimentally

determined detachment energies of pBQ$^-$.[8] The ADE is indicated in Figure 1 as the vertical dashed line.

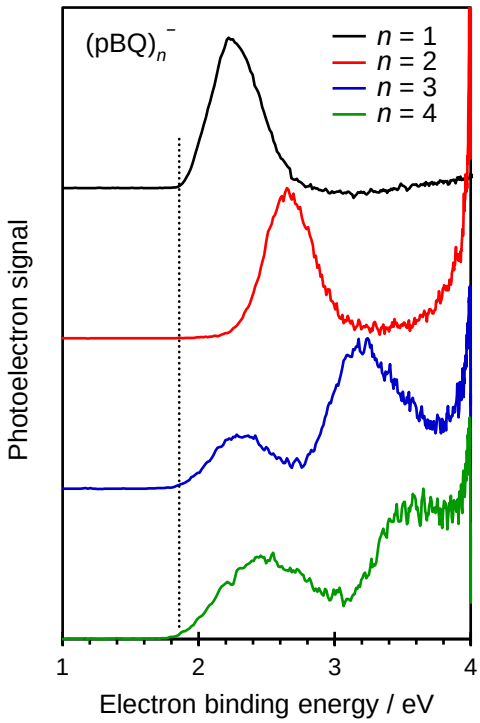

Figure 1 Photoelectron spectra of (pBQ)$_n^-$ (n = 1 - 4); n = 2 to 4 were taken at $h\nu$ = 4.00 eV and n = 1 at $h\nu$ = 4.20 eV. Each spectrum has been area normalised and offset vertically for clarity. The vertical dashed line indicates the adiabatic binding energy for pBQ$^-$.

Figure 1 also shows the photoelectron spectra of the clusters, (pBQ)$_n^-$ (n = 2 – 4). The photoelectron spectrum of the dimer has a very similar appearance as that of the monomer, but blue-shifted by ~ 0.4 eV. The trimer and tetramer show similar bands with similar successive increases in binding energy. These peaks can be assigned to direct detachment into the continuum. The VDE can be extracted from these spectra as done for the monomer and the incremental shift in the VDEs of (pBQ)$_n^-$ are plotted in Figure 2. By inspection of Figure 1, assigning the ADE is only possible for the monomer and dimer as photoelectron signal obscures the direct detachment peak onset for n = 3 and 4.

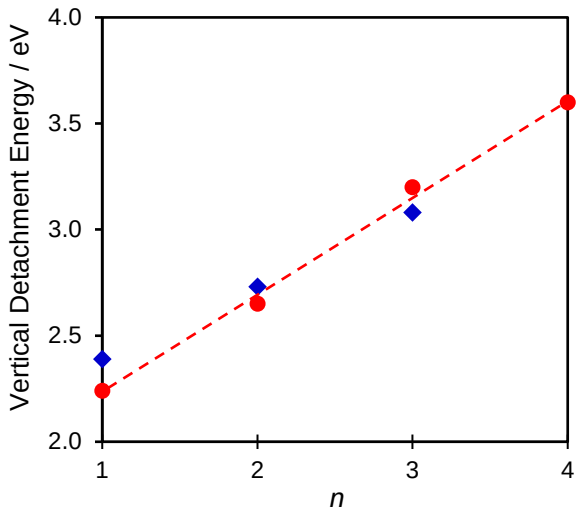

Figure 2 The trend in vertical detachment energies (VDE) of $(p\text{BQ})_n^-$ with cluster size, determined from experiment (red circles) and theory (blue diamonds). The dashed lined is a guide to the eye for the experimental trend in VDE.

In addition to the blue-shifting direct detachment band, a feature peaking at zero kinetic energy (eBE = $h\nu$ = 4.00 eV) is present in the spectra for all values of $n > 1$. Moreover, the spectral profile of these narrow peaks is featureless and has an exponential spectral profile. Near-zero kinetic energy peaks that have a Boltzmann-like energy distribution are typically signatures of thermionic (statistical) electron emission.[49–51] To observe such features requires the formation of a hot electronic ground state (with internal energy in excess of the electron binding energy) following the interaction with a photon. Hence, the observation of thermionic emission suggests that at $h\nu$ = 4.00 eV, a resonance is excited in the clusters that ultimately leads to some ground state products, which emit electrons on a longer (typically μs) timescale.

Perhaps the most striking features in Figure 1 are the photoelectron peaks in $(p\text{BQ})_3^-$ and $(p\text{BQ})_4^-$ at *lower* binding energy than the direct detachment peak for these clusters. Clearly visible are broad features at eBE ≈ 2.37 and 2.50 eV in $(p\text{BQ})_3^-$ and $(p\text{BQ})_4^-$,

respectively. By inspection Figure 1, the energies of the red-shifted peaks are similar to the direct detachment peaks present in the spectrum of the monomer. This is most clearly the case for $n = 3$ although the lower binding energy peak appears slightly blue-shifted and broadened compared to the monomer. For $n = 4$, the peak is significantly broader and blue-shifted and appears to encompass both the monomer and dimer photoelectron spectra.

B. Computational

The DFT optimised ground state geometry of *p*BQ$^-$ corresponds to a planar structure with D_{2h} symmetry. The VDE of *p*BQ$^-$ was computed to be 2.39 eV. This value is in agreement with the DFT computed energy previously reported by Stockett and Nielsen[6] and lies within ~ 0.2 eV of the experimental value determined here.

The conjugated nature of *p*BQ gives rise to a π-electron cloud capable of engaging in π-stacking. Additionally, *p*BQ can also partake in hydrogen bonding through its *para*-oxygen atoms. The balance between these non-covalent interactions can lead to structural ambiguity regarding its anionic oligomers. In order to address this, AMBER minimisation calculations were performed on (*p*BQ)$_2^-$ and five possible configurations of the dimer were identified (Figure 3). Two of these configurations appeared to be structurally identical, only differentiable by a small rotation of a single ring and the resulting minor difference in the AMBER minimisation energy (0.3 meV). As such, these configurations are represented by one structural class, labelled **IV** in Figure 3.

In the case of configurations **I** and **II**, both dimers are assembled in π-stacked arrangements (sandwich and T-shaped respectively). This is in contrast to **III** and **IV**, in which the two molecules of the dimer are associated predominantly through hydrogen bonding interactions.

DFT calculations commencing from the five AMBER configurations indicated that the π-stacked structures, **I** and **II**, were the most stable (relative energies (meV) are given in parentheses in Figure 3). Finer geometrical changes in the overall structures of **I** and **II** were noted following the DFT energy minimisation. The most notable of these was a buckling of the two oxygen atoms out of the plane of the *p*BQ ring. In Figure 4(a), the DFT optimised structure of the lowest energy configuration is presented for the dimer and clearly shows this out-of-plane distortion. Optimisation calculations employing the two configurations represented by **IV** converged to single structure, which was deemed the most energetically unfavourable structure. For all DFT configurations, the net charge is predominately localised on a single monomer with the other neutral monomer effectively solvating the charge. The computed VDE of the dimer is 2.73 eV and is included in Figure 2.

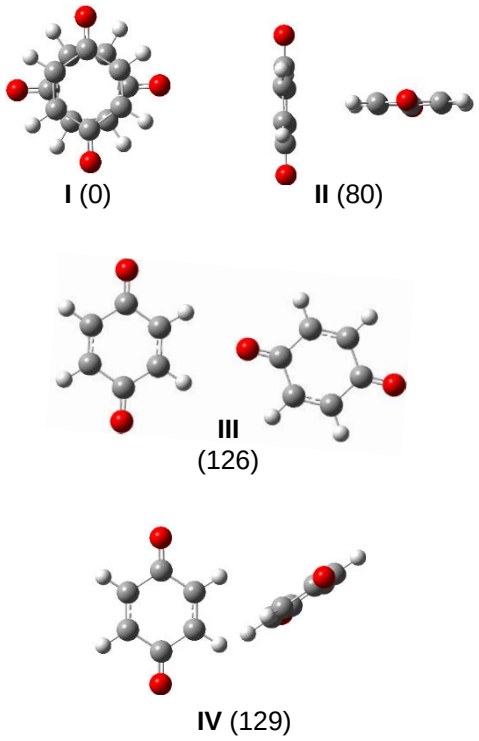

Figure 3 AMBER energy minimised configurations of $(pBQ)_2^-$. Different configurations are labelled as I – IV and their relative DFT computed optimisation energies are shown in brackets in meV.

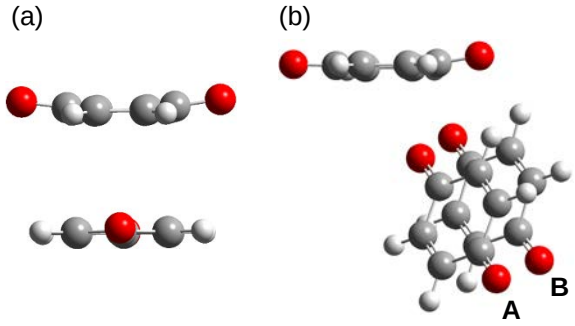

Figure 4 The minimum energy structures of (a) $(p\text{BQ})_2^-$ and (b) $(p\text{BQ})_3^-$. For the dimer, the excess charge is localised on the planar, unbuckled fragment. For the trimer, the net charge is predominantly localised on the stacked fragment labelled A.

Repeating the AMBER computational process for the trimer anion yielded 14 possible minimum energy structures. Broad similarities can be identified between a number of configurations, allowing these 14 structures to be separated into 5 overall structural classes. Geometries within each class are differentiable through fragment rotations and do not lead to significant changes in energies. In fact, DFT energy minimisations of different structures within a given class often led to a single structure. A representative geometry from each structural class for $(p\text{BQ})_3^-$ is shown in Figure 5.

DFT calculations identified class **I** structures as the most stable and the lowest energy structure for the trimer following the optimisation of class **I** is shown in Figure 4(b). Class **I** configurations consist of two π-stacked fragments in a parallel-displaced arrangement, with a third fragment held in place by a combination of quadrupole-quadrupole and hydrogen bonding interactions. Similar to the dimer, the charge in the class **I** structure is largely localised on one of the π-stacked monomers. DFT geometry optimisations of the class **I** configuration resulted in significant structural changes, including a translational shift of the unstacked fragment and a significant rotation of the π-stacked fragments, although their

parallel-displaced arrangement was retained (cf. Figure 4(b) and Figure 5). Much like the dimer, the hydrogen-bonded monomer buckles out of the plane of the quinone ring, as also previously noted in the $(pTQ)_3^-$ study.[37] The calculated VDE of the trimer is 3.08 eV and has been included in Figure 2.

Due to computational expense associated with the DFT optimisations and the additional ambiguity in assigning structures, the lowest energy structure of $(pBQ)_4^-$ has not been computed.

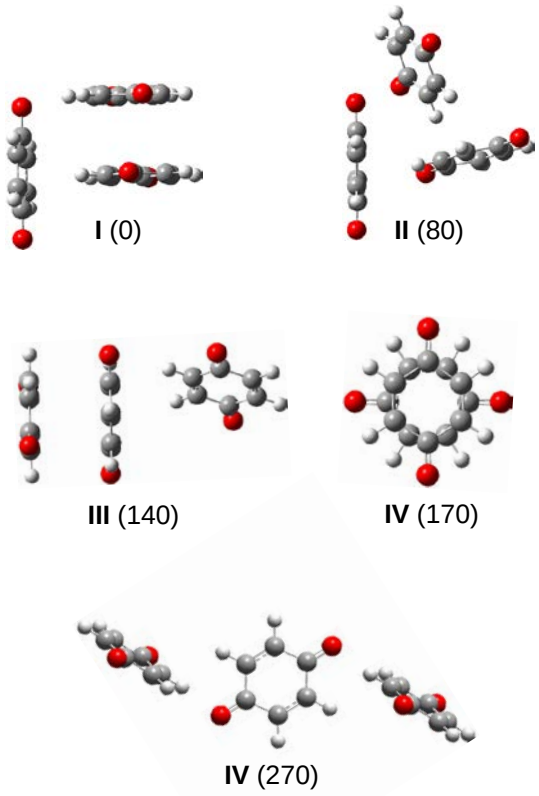

Figure 5 AMBER energy minimised configurations of $(pBQ)_3^-$. Different configuration classes are labelled as I – IV and their relative DFT computed optimisation energies are shown in brackets in meV.

IV. Discussion

A. Vertical detachment energies and cluster structures

Figure 1 shows that the peak assigned to direct detachment in $(p\text{BQ})_n^-$ has a similar spectral profile to that of $p\text{BQ}^-$. As the clusters become larger, the binding energy increases. The spectral widths do not change appreciably between n = 1 and 2, but appear to become larger for n = 3 and 4, although these are also affected by the indirect features on either side of the direct detachment peak. The fact that the direct photoelectron spectra retain a similar shape suggests that the charge remains predominantly localised on one *p*BQ monomer, which is solvated by a neutral *p*BQ. This is consistent with the DFT calculations that show that the charge is predominantly localised on one monomer. In the case of the dimer, the ωB97XD computed Mulliken charges show that 93% of the net charge is localised on the non-buckled monomer. The computed charges of the trimer also show localisation but to a lesser extent, with 34% and 66% of the charge residing on the upper and lower π-stacked monomers labelled in Figure 4(b) as A and B, respectively. The wider charge distribution observed for the trimer could be attributed to the well-known delocalisation error in approximate DFT functionals, [52,53] where the charge is artificially delocalised in order to lower the energy of the system. It is well known that this error is highly sensitive to the amount of exact exchange. For comparative purposes, Mulliken charges of the trimer were also computed using Hartree Fock (HF) and BLYP, which represent the extreme cases of 100% and 0% exact exchange, respectively. HF/6-31+G* calculations showed enhanced localisation (94% of the excess charge on A), while BLYP led to essentially equal amounts on the dimer (55% on A), illustrating the sensitivity to the amount of exchange. As such, it is difficult to quantify the charge distribution, but from these results a degree of localisation can be inferred.

The increase in VDE with each successive n can be explained in terms of the strength of the intermolecular binding present in the oligomer complexes. As the size of the anion clusters increase, so too does the number intermolecular electrostatic interactions, resulting in stronger binding for larger n. The interactions in the anions are generally stronger than in the

neutral because of the charge-induced electrostatic interactions. Hence, the cohesion energy in the anions is higher than in the neutral such that an incremental increase in VDE is observed with *n*. The computed VDEs are in good agreement with the experimentally determined energies, lying < 0.2 eV of the experimental values in all cases. Moreover, as shown in Figure 2, the overall trend is well captured qualitatively. However, the quantitative gradient of VDE(*n*) appears to be slightly underestimated.

Overall, the cluster structures determined by the calculations appear reasonable. Our only experimental probe for the structure is the photoelectron spectra and the VDE that can be extracted from these. Comparison of the computed and measured VDEs shows that they are in reasonable agreement. However, we note that the calculation of VDEs for different cluster structures and even in different cluster structure classes for the trimer leads to broadly similar VDEs. This is not wholly surprising given the fact that the charge is mostly localised in all clusters. Hence, there is some ambiguity about which structures are actually present in the ion packet under experimental conditions. In particular, because there are several structures that are relatively close in energy and lead to similar VDEs, a number of structures may be contributing to the ion packet for $n = 3$ and 4. This may in turn explain the broadening observed in the direct detachment peak for these two clusters. Nevertheless, we do expect relatively cold clusters as the electron attachment occurs at the throat of the expansion and most of the supersonic cooling occurs beyond this point. Note that we also see evidence of Ar clusters in the mass-spectrum indicating efficient overall cooling.

B. Dynamics of resonances

Present in the photoelectron spectra of $n = 3$ and 4 are additional features at eBE = ~2.37 and 2.50 eV, respectively. These bands could arise from different cluster geometries.

However, as all reasonable structures generally give broadly similar VDEs, this seems very unlikely. Instead, for all clusters studied here, $h\nu$ = 4.00 eV appears to excite a resonance in the systems as evidenced by the slow (thermionic) electrons being emitted. The photodetachment cross section measured by Brauman and coworkers shows that a broad resonance is present around *p*BQ$^-$ at 4 eV,[24] which can be assigned to a higher-lying $^2B_{3u}$ state. However, for the monomer, this resonance does not lead to an observable change in the photoelectron spectrum and the 2D photoelectron spectrum showed no evidence for ground state reformation following excitation to this resonance.[9] Given the evidence that the charge remains localised predominantly on a single *p*BQ within the clusters, it is reasonable to suggest that this same resonance is excited in the clusters. The lower binding energy features seen in the n = 3 and 4 photoelectron spectra are likely due to dynamics of this resonance in the cluster. By inspection of Figure 1, the indirect photoelectron features appear to be at similar energies as that for the monomer, *p*BQ$^-$. Specifically, if the ADE is traced down from *p*BQ$^-$ to (*p*BQ)$_3^-$ and (*p*BQ)$_4^-$, as shown by the dashed line in Figure 1, then it is clear that this lines up well with the ADEs of the indirect features. Hence, we propose that these features arise from the detachment of the monomer following excitation of the cluster. This would of course require a dissociative process upon excitation to the resonance. The appearance of the monomer would then require two photons.

Using the example of the (*p*BQ)$_3^-$, the proposed mechanism is given in Scheme 1. Absorption of the first photon by the cluster anion leads to excitation to a resonance after which, photodissociation ensues, forming the charged monomer and neutral dimer species (or complete dissociation into 3 monomers with one carrying the excess negative charge). The absorption of a second photon by *p*BQ$^-$ then generates the neutral monomer that is observed in the photoelectron spectrum of (*p*BQ)$_3^-$.

$$(p\mathrm{BQ})_3^- \xrightarrow{h\nu} [(p\mathrm{BQ})_3^-]^* \longrightarrow (p\mathrm{BQ})_{\mathrm{hot}}^- + (p\mathrm{BQ})_2$$
$$(p\mathrm{BQ})_{\mathrm{hot}}^- \xrightarrow{h\nu} p\mathrm{BQ} + \mathrm{e}^- \quad (1)$$

For both photons to be absorbed, the dynamics leading to dissociation must be on a timescale less than the laser pulse duration, which is ~ 5 ns. Excited state dissociation would unquestionably be faster. However, internal conversion of the resonance to form the ground state could also lead to dissociation because the 4 eV total energy imparted into the cluster is well above its binding energy. We note that the presence of thermionic emission evidences ground state reformation, so this is a possible mechanism. However, we cannot say whether thermionic emission is from the ground state of the cluster anion or from the monomer anion as there would be sufficient energy for either to lead to thermionic emission. From the spectral width in Figure 1, the direct detachment from the $p\mathrm{BQ}^-$ fragment following $(p\mathrm{BQ})_3^-$ dissociation is significantly broadened with respect to the photoelectron spectrum of $p\mathrm{BQ}^-$. This highlights that the $p\mathrm{BQ}^-$ fragment produced has a large amount of internal energy. The spectral blue-shift of the binding energy then suggests a differing Franck-Condon profile at higher internal energies and we do observe also that the ADE is slightly shifted to lower energies, presumably because of hot band contributions to the photoelectron spectrum. Ultimately, it is not possible to ascertain with certainty whether photodissociation of the anion cluster occurs on the resonance or following internal conversion to the ground state of the anion. This could potentially be probed by time-resolved photoelectron spectroscopy, but these experiments are beyond the scope of this work.

For $(p\mathrm{BQ})_4^-$, there is a further increase of spectral width as well as an increase in binding energy associated with the detachment band from the fragment. The increased width is not likely to be due to an increase in the internal energy of the $p\mathrm{BQ}^-$ fragment as there are now more modes and the tetramer has a broadly similar binding energy as for $(p\mathrm{BQ})_3^-$.

Instead, the much-increased width suggests that there may be other products of the photodissociation. Specifically, Figure 1 shows a significant broadening of the indirect peak indicating that two components are required to reproduce the spectral shape and suggest that both the anionic monomer and dimer are produced in the dissociation process. As with the dissociation of the trimer, the width suggests that the fragments are produced with a large amount of internal energy. Nevertheless, the $(p\mathrm{BQ})_2^-$ fragment appears to survive the dissociation on the timescale of ~5 ns. Our experiments cannot determine which fragment is dominant because of the unknown timescales involved in the process and the fixed laser pulse duration. Finally, we comment that a power dependence of the indirect versus direct detachment signals would have been useful as a further confirmation of the above assignment, but our signal levels were too low to convincingly do this.

The experimental and computational results reveal similarities between $(p\mathrm{BQ})_n^-$ and its methylated analogue, $(p\mathrm{TQ})_n^-$.[37] The calculated minimum energy configurations of $(p\mathrm{BQ})_n^-$ bear strong resemblance to those predicted for $(p\mathrm{TQ})_n^-$, n = 2 and 3. In both cases, the anion clusters adopt predominantly π-stacked arrangements, with both molecules exhibiting out-of-plane buckling of one monomer and charge localisation. For n = 3, both molecules adopt a parallel-displaced stacked arrangement with a third, hydrogen bonded monomer assembled in a distorted T shape. Similarly, the cohesion energy between the two clusters is broadly similar suggesting that the methyl group has a minor impact. In contrast, the anionic dimer of coenzyme Q_0, $(\mathrm{CQ_0})_2^-$, which has two additional methoxy groups on the ring side opposite to the methyl in *p*TQ, has a cohesion energy of ~1.0 eV for the dimer.[54] This increased binding can be correlated to the ability of $(\mathrm{CQ_0})_2^-$ to form additional hydrogen bonds.

Some of the commonalities between $(p\mathrm{BQ})_n^-$ and $(p\mathrm{TQ})_n^-$ also extend to their spectroscopic properties. Dissociation was also observed in $(p\mathrm{TQ})_2^-$. Comita and Brauman

identified a bound state at 1.9 eV, which dissociated to form the monomer anion that was observed in the experiment.[24] Dissociation was also inferred from photoelectron spectra following excitation of resonances at $h\nu \sim 3$ eV.[37] However, poor signal-to-noise meant that we could not explore the photoelectron spectroscopy of the $(p\mathrm{TQ})_2^-$ at $h\nu = 4.00$ eV as probed here. In contrast, $(p\mathrm{TQ})_3^-$ did not show evidence of dissociation, including at $h\nu \sim 4$ eV. Instead, for $2.5 < h\nu < 3.4$ eV, internal conversion to form a non-valence state was observed.[38] The same mechanism was also observed in $(\mathrm{CQ}_0)_2^-$ around the detachment threshold,[54] which also did not show dissociation at $h\nu \sim 4$ eV.

Unfortunately, we could only conduct the present experiments at a single photon energy. It would be interesting to perform 2D photoelectron spectroscopy to probe the photon energy dependence of the dissociation, similar to the dissociation we previously observed in *p*-dinitrobenzene,[55] but this would require much higher signal levels than are currently attainable.

V. Conclusion

In conclusion, we have presented the photoelectron spectroscopy of *p*-benzoquinone cluster anions, $(p\mathrm{BQ})_n^-$, with $n = 1 - 4$ at $h\nu \approx 4.00$ eV together with calculations aimed at identifying possible structures. The spectra reveal that the vertical detachment energy of the clusters increases incrementally by ~ 0.4 eV, which can be explained in terms of the cohesion energy of the cluster. Electronic structure calculations identify the most probable structure for $(p\mathrm{BQ})_2^-$, while for $(p\mathrm{BQ})_3^-$, a number of structures are possible and will likely contribute to the spectrum. The predicted structures are consistent with those calculated for related quinone clusters. For all clusters, thermionic emission is observed suggesting that resonances are excited at $h\nu = 4.00$ eV, leading to the formation of ground state anions with large amounts of

excess energy. For n = 3 and 4, fragmentation is additionally observed in the spectra with signatures of photodetachment from the monomer anion for n = 3 and the monomer and dimer anions for n = 4. Our results show the complex dynamics occurring in these relatively simple clusters, despite the accessed excited states lying energetically in the detachment continuum.

Acknowledgements

G M-B would like to thank EPSRC for the award of a DTP studentship (grant EP/M507854/1). The authors would like to thank Aude Lietard and Andrew Christy for many insightful discussions and Durham University for the use of its high performance computing facility, Hamilton.

References

[1] H. Nohl, W. Jordan, and R.J. Youngman, Adv. Free Radic. Biol. Med. **2**, 211 (1986).

[2] N. El-Najjar, H. Gali-Muhtasib, R.A. Ketola, P. Vuorela, A. Urtti, and H. Vuorela, Phytochem. Rev. **10**, 353 (2011).

[3] S. Fukuzumi, Bull. Chem. Soc. Jpn. **79**, 177 (2006).

[4] S.D. Minteer, F. Giroud, R.D. Milton, and B. Tan, Meet. Abstr. **MA2015-01**, 2307 (2015).

[5] I. Abraham, R. Joshi, P. Pardasani, and R.T. Pardasani, J. Braz. Chem. Soc. **22**, 385 (2011).

[6] M.H. Stockett and S.B. Nielsen, Phys. Chem. Chem. Phys. **18**, 6996 (2016).

[7] Y. Honda, M. Hada, M. Ehara, and H. Nakatsuji, J. Phys. Chem. A **106**, 3838 (2002).

[8] J. Schiedt and R. Weinkauf, J. Chem. Phys. **110**, 304 (1998).

[9] C.W. West, J.N. Bull, E. Antonkov, and J.R.R. Verlet, J. Phys. Chem. A **118**, 11346 (2014).

[10] M. Allan, Chem. Phys. **81**, 235 (1983).

[11] M. Allan, Chem. Phys. **84**, 311 (1984).

[12] C.D. Cooper, W.T. Naff, and R.N. Compton, J. Chem. Phys. **63**, 2752 (1975).

[13] L.G. Christophorou, J.G. Carter, and A.A. Christodoulides, Chem. Phys. Lett. **3**, 237 (1969).

[14] P.M. Collins, L.G. Christophorou, E.L. Chaney, and J.G. Carter, Chem. Phys. Lett. **4**, 646 (1970).

[15] K.S. Strode and E.P. Grimsrud, Chem. Phys. Lett. **229**, 551 (1994).

[16] A. Modelli and P.D. Burrow, J. Phys. Chem. **88**, 3550 (1984).

[17] R.L. Gordon, D.R. Sieglaff, G.H. Rutherford, and K.L. Stricklett, Int. J. Mass Spectrom. Ion Process. **164**, 177 (1997).

[18] S.A. Pshenichnyuk, G.S. Lomakin, A.I. Fokin, I.A. Pshenichnyuk, and N.L. Asfandiarov, Rapid Commun. Mass Spectrom. RCM **20**, 383 (2006).

[19] N.L. Asfandiarov, S.A. Pshenichnyuk, A.I. Fokin, and E.P. Nafikova, Chem. Phys. **298**, 263 (2004).

[20] M.O.A. El Ghazaly, A. Svendsen, H. Bluhme, S.B. Nielsen, and L.H. Andersen, Chem. Phys. Lett. **405**, 278 (2005).

[21] A.I. Lozano, J.C. Oller, D.B. Jones, R.F. da Costa, M.T.D.N. Varella, M.H.F. Bettega, F.F. da Silva, P. Limão-Vieira, M.A.P. Lima, R.D. White, M.J. Brunger, F. Blanco, A. Muñoz, and G. García, Phys. Chem. Chem. Phys. **20**, 22368 (2018).

[22] G. Mensa-Bonsu, A. Lietard, and J.R.R. Verlet, Phys. Chem. Chem. Phys. (2019).

[23] Q. Fu, J. Yang, and X.-B. Wang, J. Phys. Chem. A **115**, 3201 (2011).

[24] P.B. Comita and J.I. Brauman, J. Am. Chem. Soc. **109**, 7591 (1987).

[25] J. Marks, P.B. Comita, and J.I. Brauman, J. Am. Chem. Soc. **107**, 3718 (1985).

[26] J. Weber, K. Malsch, and G. Hohlneicher, Chem. Phys. **264**, 275 (2001).

[27] R. Pou-Amérigo, L. Serrano-Andrés, M. Merchán, E. Ortí, and N. Forsberg, J. Am. Chem. Soc. **122**, 6067 (2000).

[28] A.A. Kunitsa and K.B. Bravaya, J. Phys. Chem. Lett. **6**, 1053 (2015).

[29] A. Loupas and J.D. Gorfinkiel, Phys. Chem. Chem. Phys. **19**, 18252 (2017).

[30] A.A. Kunitsa and K.B. Bravaya, Phys. Chem. Chem. Phys. **18**, 3454 (2016).

[31] R.F. da Costa, J.C. Ruivo, F. Kossoski, M.T.D.N. Varella, M.H.F. Bettega, D.B. Jones, M.J. Brunger, and M.A.P. Lima, J. Chem. Phys. **149**, 174308 (2018).

[32] N. Hayashi, T. Yoshikawa, T. Ohnuma, H. Higuchi, K. Sako, and H. Uekusa, Org. Lett. **9**, 5417 (2007).

[33] P.J. O'Malley, Chem. Phys. Lett. **274**, 251 (1997).

[34] C.S. Anstöter, J.N. Bull, and J.R.R. Verlet, Int. Rev. Phys. Chem. **35**, 509 (2016).

[35] D.A. Horke, Q. Li, L. Blancafort, and J.R.R. Verlet, Nat. Chem. **5**, 711 (2013).

[36] H.-Y. Cheng and Y.-S. Huang, Phys. Chem. Chem. Phys. **16**, 26306 (2014).

[37] J.N. Bull and J.R.R. Verlet, Phys. Chem. Chem. Phys. **19**, 26589 (2017).

[38] J.N. Bull and J.R.R. Verlet, Sci. Adv. **3**, e1603106 (2017).

[39] J.P. Rogers, C.S. Anstöter, J.N. Bull, B.F.E. Curchod, and J.R.R. Verlet, J. Phys. Chem. A **123**, 1602 (2019).

[40] U. Even, J. Jortner, D. Noy, N. Lavie, and C. Cossart-Magos, J. Chem. Phys. **112**, 8068 (2000).

[41] W.C. Wiley and I.H. McLaren, Rev. Sci. Instrum. **26**, 1150 (1955).

[42] A.T.J.B. Eppink and D.H. Parker, Rev. Sci. Instrum. **68**, 3477 (1997).

[43] D.A. Horke, G.M. Roberts, J. Lecointre, and J.R.R. Verlet, Rev. Sci. Instrum. **83**, 063101 (2012).

[44] G.M. Roberts, J.L. Nixon, J. Lecointre, E. Wrede, and J.R.R. Verlet, Rev. Sci. Instrum. **80**, 053104 (2009).

[45] D.A. Case, T.E. Cheatham, T. Darden, H. Gohlke, R. Luo, K.M. Merz, A. Onufriev, C. Simmerling, B. Wang, and R.J. Woods, J. Comput. Chem. **26**, 1668 (2005).

[46] J. Wang, R.M. Wolf, J.W. Caldwell, P.A. Kollman, and D.A. Case, J. Comput. Chem. **25**, 1157 (2004).

[47] J.-D. Chai and M. Head-Gordon, Phys. Chem. Chem. Phys. **10**, 6615 (2008).

[48] M. Frisch, G. Trucks, H. Schlegel, G. Scuseria, M. Robb, J. Cheeseman, G. Scalmani, V. Barone, B. Mennucci, G. Petersson, H. Nakatsuji, M. Caricato, X. Li, H. Hratchian, A. Izmaylov, J. Bloino, G. Zheng, J. Sonnenberg, M. Hada, M. Ehara, K. Toyota, R. Fukuda, J. Hasegawa, M. Ishida, T. Nakajima, Y. Honda, O. Kitao, H. Nakai, T. Vreven, J. Montgomery, J. Peralta, F. Ogliaro, M. Bearpark, J. Heyd, E. Brothers, K. Kudin, V. Staroverov, R. Kobayashi, J. Normand, K. Raghavachari, A. Rendell, J. Burant, S. Iyengar, J. Tomasi, M. Cossi, N. Rega, J. Millam, M. Klene, J. Knox, J. Cross, V. Bakken, C. Adamo, J. Jaramillo, R. Gomperts, R. Stratmann, O. Yazyev, A. Austin, R. Cammi, C. Pomelli, J. Ochterski, R. Martin, K. Morokuma, V. Zakrzewski, G. Voth, P. Salvador, J. Dannenberg, S. Dapprich, A. Daniels, Farkas, J. Foresman, J. Ortiz, J. Cioslowski, and D. Fox, Gaussian 09 Gaussian Inc Wallingford CT (2009).

[49] E.E.B. Campbell, G. Ulmer, and I.V. Hertel, Phys. Rev. Lett. **67**, 1986 (1991).

[50] A. Amrein, R. Simpson, and P. Hackett, J. Chem. Phys. **94**, 4663 (1991).

[51] O.W. Richardson, *On the Negative Radiation from Hot Platinum* (Proc. Cambridge Philos. Soc., 1901).

[52] A.J. Cohen, P. Mori-Sánchez, and W. Yang, Science **321**, 792 (2008).

[53] D. Hait and M. Head-Gordon, J. Phys. Chem. Lett. **9**, 6280 (2018).

[54] J.N. Bull, C.W. West, and J.R.R. Verlet, Chem. Sci. **7**, 5352 (2016).

[55] C.S. Anstöter, T.E. Gartmann, L.H. Stanley, A.V. Bochenkova, and J.R.R. Verlet, Phys. Chem. Chem. Phys. **20**, 24019 (2018).